

The stick-slip decomposition method for modeling large-deformation Coulomb frictional contact

Layla K. Amaireh¹ and Ghadir Haikal^{*2}

¹*Applied Science Private University, Amman, Jordan*

²*Lyles School of Civil Engineering, Purdue University, West Lafayette, Indiana, USA*

(Received May 24, 2018, Revised June 22, 2018, Accepted June 23, 2018)

Abstract. This paper discusses the issues associated with modeling frictional contact between solid bodies undergoing large deformations. The most common model for friction on contact interfaces in solid mechanics is the Coulomb friction model, in which two distinct responses are possible: stick and slip. Handling the transition between these two phases computationally has been a source of algorithmic instability, lack of convergence and non-unique solutions, particularly in the presence of large deformations. Most computational models for frictional contact have used penalty or updated Lagrangian approaches to enforce frictional contact conditions. These two approaches, however, present some computational challenges due to conditioning issues in penalty-type implementations and the iterative nature of the updated Lagrangian formulation, which, particularly in large simulations, may lead to relatively slow convergence. Alternatively, a plasticity-inspired implementation of frictional contact has been shown to handle the stick-slip conditions in a local, algorithmically efficient manner that substantially reduces computational cost and successfully avoids the issues of instability and lack of convergence often reported with other methods (Laursen and Simo 1993). The formulation of this approach, however, has been limited to the small deformations realm, a fact that severely limited its application to contact problems where large deformations are expected. In this paper, we present an algorithmically consistent formulation of this method that preserves its key advantages, while extending its application to the realm of large-deformation contact problems. We show that the method produces results similar to the augmented Lagrangian formulation at a reduced computational cost.

Keywords: frictional contact; Coulomb model; large deformations

1. Introduction

The computational modeling of a large class of contact problems involves simulating frictional conditions on contact interfaces in composite materials, laminate and layered structures and soil-structure interaction in underground piles, pipes and tunnels. The most common model for friction on contact interfaces in solid mechanics is the Coulomb, or dry friction behavioral model, which allows for two distinct states: a stick state, in which two points in contact are glued together, and no motion tangential to the contact surface occurs, and

*Corresponding author, Assistant Professor, Email: ghaikal@purdue.edu

a slip state when the bodies can slide freely with respect to each other while the tangential interface traction remains constant. The first state occurs when the ratio between the tangential and normal components of interface tractions at the contact location is less than a material-specific value, called the Coulomb friction coefficient. When the tangential traction reaches the Coulomb limit, resistance to transverse sliding is released, and the ratio between the tangential and normal components of interface tractions is assumed to remain equal to the friction coefficient.

In the computational modeling of two bodies in contact using the finite element method, it is critical for the computational model to reflect interface conditions accurately. Normal contact constraints are enforced to prevent non-admissible overlap or mass inter-penetration, while tangential frictional conditions distinguish between the stick and slip states within each load step. The stick state requires enforcing additional constraints preventing motion tangential to the contact plane, while the slip state involves free tangential motion under constant tangential force. Lateral stick conditions can be enforced using the same approaches used for normal contact constraints, namely the penalty, Lagrange multiplier, or Augmented Lagrangian methods (Wriggers 2006). The Lagrange multiplier can be applied at a set of discrete contact locations, or interpolated along the interface (McDevitt and Laursen 2000, Puso and Laursen 2004, Baillet and Sassi 2005, Fischer and Wriggers 2006). While the Lagrange multiplier approach enforces exact stick conditions, it introduces a dual unknown force, therefore increasing the size of the problem, invoking stability concerns regarding dual discretizations, and leading to scaling-related convergence difficulties (Vulovic *et al.* 2007, Gu *et al.* 2009). Alternatively, the penalty method simulates stick conditions by controlling lateral sliding at contact locations through a user-defined, arbitrarily large penalty parameter. The challenge in using the penalty method, however, is in identifying the magnitude of the penalty parameter: A large parameter is needed to preclude sliding. Arbitrarily large values, however, could potentially lead to ill-conditioning and instability (Vulovic *et al.* 2007 and Ștefancu *et al.* 2011). These numerical issues are particularly pronounced when the penalty approach is used for both normal and tangential conditions. The Augmented Lagrangian method (Alart and Curnier 1991) combines the benefits of the penalty and Lagrangian multiplier approaches, and the contact force is computed through an iterative process starting with a penalty-based estimate. This method has the advantage of obtaining the exact Lagrange multiplier values and avoiding the numerical problems associated with the penalty approach (Simo and Laursen 1992, Laursen and Simo 1993a, Wriggers and Zavarise 1993, and Pietrzak and Curnier 1999). It remains, however, an iterative process that, similar to the Lagrange multiplier approach, requires an initial assumption of stick/slip at each contact point.

When the above methods are used to enforce Coulomb frictional conditions, an assumption has to be made at the onset of the simulation whether contact at a given point is in a state stick or slip. If a stick condition is assumed, the lateral force required to enforce zero tangential displacement is computed. This assumption has to be revisited at the end of the analysis. If the tangential force is found to be in excess of the Coulomb frictional limit, defined as the normal force multiplied by the surface friction coefficient, the stick condition is released to allow free tangential slip while the tangential force is kept at the Coulomb limit, and the overall solution is repeated under the revised assumption. For large meshes, and under material and/or geometric nonlinearity, this process requires multiple repetitions of the solution of the global nonlinear equilibrium equations for the coupled system. Furthermore, since the Coulomb limit changes with variations in the normal contact force, it is common for nodes to oscillate between stick and slip conditions throughout the analysis. The change in stick/slip conditions at multiple contact nodes could be the source of lack of convergence or instability, with nodes going in- and out-of contact, and oscillating between

stick and slip states (Sheng *et al.* 2006).

An alternative approach to enforcing frictional contact conditions is based on an analogy between the formulation and implementation of the constitutive equations for friction and rate-independent elasto-plasticity (Ibrahimbegovic and Wilson 1991, Laursen and Simo 1993b). In small-deformation elasto-plasticity theory, the strains are decomposed into elastic (reversible) and inelastic (irreversible) components. Stresses are accrued linearly with increasing strains until the elasticity limit, defined by a stress yield surface, is reached. Once the material enters the plasticity range, stresses are computed through a return mapping algorithm that ensures that the yield surface limits for stress are not exceeded while plastic strains can increase indefinitely through plastic flow. In the absence of hardening, stresses are therefore bound by their magnitude at maximum elastic strain. Plastic strain flow is governed by a rate-independent plasticity parameter and occurs in a direction determined by a plastic energy functional. It is common to assume an associative flow rule, under which plastic strains flow orthogonal to the yield surface.

A number of parallels can be drawn between elasto-plasticity and Coulomb frictional contact; the tangential displacement can be thought of as comprising of elastic or reversible (stick) and plastic or irreversible (slip) components. The tangential traction forces can accrue linearly in the stick phase, and are computed as the forces required to enforce the stick, or zero relative transverse motion, condition. When these forces reach the maximum value allowed by the Coulomb model, lateral displacement occurs through “plastic” slip and the tangential traction is computed through a return mapping algorithm with an appropriate flow rule for the tangential displacement. Lateral tractions are bound by their maximum stick value, with no increases allowed during “plastic” slip. The flow of slip deformations is controlled through an internal variable that can be calculated at the material point level without interfering with the global solution. Perfect stick conditions can be achieved by enforcing zero tangential deformations on the stick component only. The separation between stick and slip tangent displacements enables the enforcement of this condition on the stick component regardless of whether the total tangential displacement is in a stick or slip state.

The stick-slip decomposition method eliminates the need for repeated solutions of the nonlinear system of global equilibrium equations to enforce and release lateral contact constraints, therefore reducing the associated potential convergence problems. This method was implemented effectively in the context of small-deformation elasticity, and results showed that the stick-slip decomposition enables a smooth transition between stick and slip states without causing numerical oscillations or instability (Laursen and Simo 1993b). Its application in the context of large deformations, however, has proven to be a challenge (Sheng *et al.* 2006, Masud *et al.* 2012), and recent works on frictional contact in the presence of large deformations remain reliant on the penalty-based Augmented Lagrangian (Busetta *et al.* 2012, Gholami *et al.* 2016, Burman *et al.* 2017, Galvez *et al.* 2017) or Nitsche (Mlika *et al.* 2017) approaches, and mixed methods (Hild and Renard 2010, Popp *et al.* 2012, among many others).

The main issue with implementing the stick-slip decomposition method for large-deformation frictional contact is due to the fact that, given the nonlinear relationship between the displacements and strains, an additive decomposition of the tangential displacement field does not translate into a linear decomposition of interface strain and stress fields. Consequently, isolating the component of the traction responsible for maximum “stick” for the purpose of defining a yield surface and detecting the onset of “slip” is not readily obvious. This problem was resolved in large-deformation elasto-plasticity by adopting a multiplicative decomposition

of the strain field that induces a similar decomposition of stress. This approach, however, is not applicable to the frictional contact problem since the zero-stick condition needs to be applied directly to the displacement, not strain, field.

In this paper we discuss the formulation of the frictional contact problem for the case of large-deformation hyperelasticity and propose a new approach for extending the stick-slip decomposition to frictional contact in the presence of large deformations. Numerical implementation shows that the proposed approach is very effective at ensuring a smooth transition between stick and slip states at a much reduced computational cost. The outline of the paper is as follows: In Section 2, we outline the formulation of the frictional contact problem, starting with the governing equations for coupled systems (Section 2.1), energy formulation (Section 2.2) and finite element discretization (Section 2.3). Section 2.4 describes standard approaches for enforcing normal and tangential contact conditions. The issues surrounding the handling of stick/slip transitions are discussed and the stick-slip decomposition approach for small-deformation frictional contact is presented in Section 2.5. Section 2.6 discusses the challenges associated with the extension of this method to the case of large deformations, and the proposed methodology is described in Section 3. Numerical examples are presented and discussed in Section 4 and the conclusions are summarized in Section 5.

2. Formulation

We begin our presentation of the governing equations for the frictional contact problem with a short overview of the formulation of a coupled problem where two bodies meet through an interface. We discuss the conditions needed to enforce full geometric compatibility and a complete transfer of tractions for the fully coupled system, and then discuss how the formulation can be modified to account for the specifics of unilateral contact and frictional conditions according to the Coulomb model.

2.1 Equilibrium and virtual work

Consider the two solid domains in contact, Ω^1 and Ω^2 shown in Fig. 1. The boundary Γ of each domain can be divided into three parts $\Gamma = \Gamma_t \cup \Gamma_u \cup \Gamma_c$ where Γ_t and Γ_u denote the Neumann and Dirichlet parts of that boundary, respectively, and Γ_c refers to the contact interface. Note that $\Gamma_t \cap \Gamma_u \cap \Gamma_c = \emptyset$ in each body.

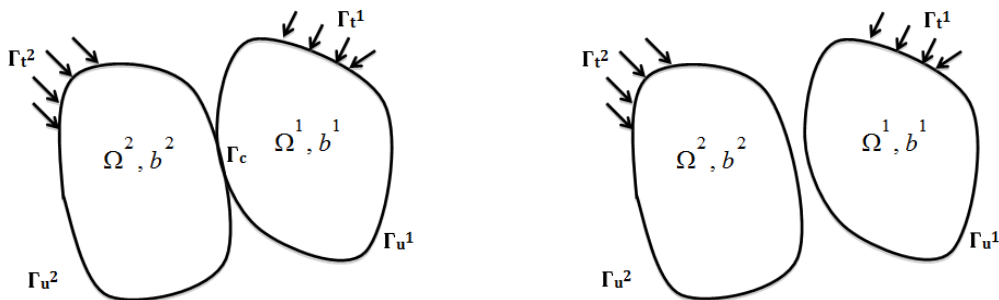


Fig. 1 Two Solid Domains in No Contact (Left) and Contact Configurations (Right)

Given the body force vector field for each solid \mathbf{b}^1 and \mathbf{b}^2 , prescribed traction fields \mathbf{t}^1 and \mathbf{t}^2 on Γ_t^1 and Γ_t^2 , and prescribed displacement fields \mathbf{g}^1 and \mathbf{g}^2 on Γ_u^1 and Γ_u^2 , respectively, the strong form of the governing equations in each of the two domains can be stated as follows

$$\begin{aligned} \operatorname{div} \boldsymbol{\sigma}^1 + \mathbf{b}^1 &= \mathbf{0} \text{ in } \Omega^1 & \boldsymbol{\sigma}^1 \mathbf{n}^1 &= \mathbf{t}^1 \text{ on } \Gamma_t^1 & \mathbf{u}^1 &= \mathbf{g}^1 \text{ on } \Gamma_u^1 \\ \operatorname{div} \boldsymbol{\sigma}^2 + \mathbf{b}^2 &= \mathbf{0} \text{ in } \Omega^2 & \boldsymbol{\sigma}^2 \mathbf{n}^2 &= \mathbf{t}^2 \text{ on } \Gamma_t^2 & \mathbf{u}^2 &= \mathbf{g}^2 \text{ on } \Gamma_u^2, \end{aligned} \tag{1}$$

where div is the divergence operator, $\boldsymbol{\sigma}^i$ is the Cauchy stress tensor in each body, and \mathbf{n}^i is the outer surface normal in each domain. When the two bodies are fully coupled, the conditions of displacement continuity and traction equilibrium on the interface can be expressed as

$$\mathbf{u}^1 = \mathbf{u}^2, \quad \boldsymbol{\sigma}^1 \mathbf{n}^1 + \boldsymbol{\sigma}^2 \mathbf{n}^2 = \mathbf{0} \text{ on } \Gamma_c \tag{2}$$

Note that $\mathbf{n}^1 = -\mathbf{n}^2$ on Γ_c . Defining the spaces $S = \{\mathbf{u} \in H^1(\Omega): \mathbf{u} = \mathbf{g} \text{ on } \Gamma_u\}$, $V = \{\bar{\mathbf{u}} \in H^1(\Omega): \bar{\mathbf{u}} = \mathbf{0} \text{ on } \Gamma_u\}$, in each domain, as well as $V^c = \{\bar{\mathbf{u}} \in H^{1/2}(\Gamma_c)\}$ on the interface, the weighted residual forms of Eqs. (1), (2) for the coupled problem can be written as

$$\begin{aligned} \int_{\Omega^1} (\operatorname{div} \boldsymbol{\sigma}^1 + \mathbf{b}^1) \cdot \bar{\mathbf{u}}^1 d\Omega + \int_{\Gamma^1} (\mathbf{t}^1 - \boldsymbol{\sigma}^1 \mathbf{n}^1) \cdot \bar{\mathbf{u}}^1 d\Gamma + \int_{\Omega^2} (\operatorname{div} \boldsymbol{\sigma}^2 + \mathbf{b}^2) \cdot \bar{\mathbf{u}}^2 d\Omega \\ + \int_{\Gamma^2} (\mathbf{t}^2 - \boldsymbol{\sigma}^2 \mathbf{n}^2) \cdot \bar{\mathbf{u}}^2 d\Gamma - \int_{\Gamma_c} (\boldsymbol{\sigma}^1 \mathbf{n}^1 + \boldsymbol{\sigma}^2 \mathbf{n}^2) \cdot \bar{\mathbf{u}}^c d\Gamma = 0 \end{aligned} \tag{3}$$

$$\forall \bar{\mathbf{u}}^1 \in V^1, \quad \bar{\mathbf{u}}^2 \in V^2, \quad \bar{\mathbf{u}}^c \in V^c.$$

In these equations, $\bar{\mathbf{u}}^1$ and $\bar{\mathbf{u}}^2$ are the virtual or variational displacement fields for domains Ω^1 and Ω^2 , respectively, while $\bar{\mathbf{u}}^c$ is the virtual displacement along the contact interface. Applying the divergence theorem to the terms $\operatorname{div} \boldsymbol{\sigma}^1$ on Ω^1 and $\operatorname{div} \boldsymbol{\sigma}^2$ on Ω^2 in Eq. (3) and imposing homogeneous boundary conditions on the Dirichlet part of each boundary, we obtain the symmetric form of the weighted residual of the coupled problem

$$G(\mathbf{u}, \bar{\mathbf{u}}) = G(\mathbf{u}, \bar{\mathbf{u}})^1 + G(\mathbf{u}, \bar{\mathbf{u}})^2 + G(\mathbf{u}, \bar{\mathbf{u}})^c = 0 \quad \forall \bar{\mathbf{u}}^1 \in V^1, \quad \bar{\mathbf{u}}^2 \in V^2, \quad \bar{\mathbf{u}}^c \in V^c \tag{4}$$

$$G(\mathbf{u}, \bar{\mathbf{u}})^1 = - \int_{\Omega^1} \boldsymbol{\sigma}^1 \cdot \nabla \bar{\mathbf{u}}^1 \cdot d\Omega + \int_{\Omega^1} \mathbf{b}^1 \cdot \bar{\mathbf{u}}^1 d\Omega + \int_{\Gamma^1} \mathbf{t}^1 \cdot \bar{\mathbf{u}}^1 d\Gamma \tag{5}$$

$$G(\mathbf{u}, \bar{\mathbf{u}})^2 = - \int_{\Omega^2} \boldsymbol{\sigma}^2 \cdot \nabla \bar{\mathbf{u}}^2 \cdot d\Omega + \int_{\Omega^2} \mathbf{b}^2 \cdot \bar{\mathbf{u}}^2 d\Omega + \int_{\Gamma^2} \mathbf{t}^2 \cdot \bar{\mathbf{u}}^2 d\Gamma \tag{6}$$

$$G(\mathbf{u}, \bar{\mathbf{u}})^c = \int_{\Gamma_c} \boldsymbol{\sigma}^1 \mathbf{n}^1 \cdot (\bar{\mathbf{u}}^1 - \bar{\mathbf{u}}^c) d\Gamma + \int_{\Gamma_c} \boldsymbol{\sigma}^2 \mathbf{n}^2 \cdot (\bar{\mathbf{u}}^2 - \bar{\mathbf{u}}^c) d\Gamma \tag{7}$$

in addition to the displacement continuity condition on the interface

$$\mathbf{u}^1 = \mathbf{u}^2 \text{ on } \Gamma_c \tag{8}$$

In the above equations, $G(\mathbf{u}, \bar{\mathbf{u}})^1$, $G(\mathbf{u}, \bar{\mathbf{u}})^2$ are the virtual work functionals in each of the two bodies, while $G(\mathbf{u}, \bar{\mathbf{u}})^c$ is the virtual work along the interface and $\mathbf{u} = [\mathbf{u}^1, \mathbf{u}^2]$ is the displacement field in the coupled domain.

In a primal formulation of the coupled problem, the displacement continuity condition (8) is

enforced as a Dirichlet-type condition along the interface. The variational displacement fields can be arbitrary and need not obey the continuity constraint that applies to the real field. However, it is important to note that when $\bar{\mathbf{u}}^1 = \bar{\mathbf{u}}^2 = \bar{\mathbf{u}}^c$ the interface work term $G(\mathbf{u}, \bar{\mathbf{u}})^c$ disappears and the total virtual work is the sum of the work done in each domain $G(\mathbf{u}, \bar{\mathbf{u}}) = G(\mathbf{u}, \bar{\mathbf{u}})^1 + G(\mathbf{u}, \bar{\mathbf{u}})^2$. Therefore, it can be concluded that when the virtual displacement field is continuous along the interface between the two bodies, the equilibrium of interface tractions is automatically satisfied and the transfer of tractions across the interface is complete. In standard Bubnov-Galerkin finite element formulations, the primal displacement fields are discretized via partition-of-unity interpolation functions, and this condition is satisfied by design on interfaces between elements due to the C^0 continuity of the real and variational displacement fields. When two different meshes meet across an interface, continuity constraints need to be imposed on the displacement fields to enforce displacement continuity and a complete transfer of tractions (Eq. (2)) across the interface.

Continuity conditions are enforced separately in the normal and tangential directions to prevent non-physical overlap or mass inter-penetration, and impose Coulomb frictional conditions, respectively. Assuming \mathbf{n}^i to be the surface normal to Γ_c in Ω^i , we can decompose the traction vectors on the interface into normal and tangential components as follows

$$\mathbf{t}^i = \boldsymbol{\sigma}^i \mathbf{n}^i = t_n^i \mathbf{n}^i + \mathbf{t}_T^i \quad i = 1,2, \tag{9}$$

where $\mathbf{t}_T^i = [\mathbf{I} - \mathbf{n}^i \otimes \mathbf{n}^i] \mathbf{t}^i = \mathbf{P}^i \mathbf{t}^i$ and \mathbf{P}^i is the projection tensor on side i of the interface

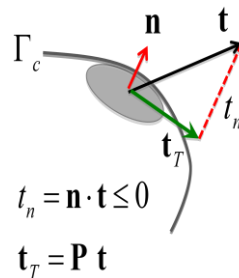


Fig. 2 Decomposition of surface tractions into normal \mathbf{t}_n and tangential \mathbf{t}_T components

Note that $\mathbf{P} \mathbf{t}_T = \mathbf{t}_T$, and therefore the projection tensor satisfies the property $\mathbf{P} \mathbf{P} = \mathbf{P}$. Similarly, the displacement field can be decomposed into normal and tangential components as follows

$$\mathbf{u}^i = u_n^i \mathbf{n}^i + \mathbf{u}_T^i \quad i = 1,2. \tag{10}$$

Taking these decompositions into account, the virtual work along the interface can also be expressed as the sum of normal and tangential contributions such that

$$\begin{aligned}
 G(\mathbf{u}, \bar{\mathbf{u}})^c = & \int_{\Gamma_c} t_n^1 (\bar{u}_n^1 - \bar{u}_n^c) d\Gamma + \int_{\Gamma_c} \mathbf{t}_T^1 \cdot (\bar{\mathbf{u}}_T^1 - \bar{\mathbf{u}}_T^c) d\Gamma + \int_{\Gamma_c} t_n^2 (\bar{u}_n^2 - \bar{u}_n^c) d\Gamma \\
 & + \int_{\Gamma_c} \mathbf{t}_T^2 \cdot (\bar{\mathbf{u}}_T^2 - \bar{\mathbf{u}}_T^c) d\Gamma
 \end{aligned} \tag{11}$$

In finite element implementations of contact problems, it is common to designate one side of the interface as ‘master’ and the other as ‘slave.’ The interface displacement field is defined to be that of the master side, which we chose to be $\bar{\mathbf{u}}^c = \bar{\mathbf{u}}^2$, the interface virtual work statement reduces to

$$G(\mathbf{u}, \bar{\mathbf{u}})^c = \int_{\Gamma_c} t_n^1 \cdot (\bar{u}_n^1 - \bar{u}_n^2) d\Gamma + \int_{\Gamma_c} \mathbf{t}_T^1 \cdot (\bar{\mathbf{u}}_T^1 - \bar{\mathbf{u}}_T^2) d\Gamma. \quad (12)$$

In this form, the normal and tangential tractions on the interface are represented by their values on the slave side of the interface, t_n^1 and \mathbf{t}_T^1 . Recognizing that $\mathbf{n} \equiv \mathbf{n}^2 = -\mathbf{n}^1$ is the normal on the master surface, we observe that $t_n^1 \cdot (\bar{u}_n^1 - \bar{u}_n^2) = (\mathbf{t}^1 \cdot \mathbf{n})[\mathbf{n} \cdot (\mathbf{u}^1 - \mathbf{u}^2)]$. We also define $g^n = \mathbf{n} \cdot (\mathbf{u}^1 - \mathbf{u}^2)$ and $\mathbf{g}^T = \mathbf{u}_T^1 - \mathbf{u}_T^2$ to be the normal and tangential compatibility conditions, measuring the relative motion of a slave node 1 with respect to its projection on the master surface 2, in the normal and tangential directions, respectively.

Dropping the superscripts and defining the interface tractions $t_n \equiv \mathbf{t}^1 \cdot \mathbf{n}$, $\mathbf{t}_T \equiv \mathbf{t}_T^1$, the total virtual work statement in the coupled system is written as follows

$$G(\mathbf{u}, \bar{\mathbf{u}}) = G(\mathbf{u}, \bar{\mathbf{u}})^1 + G(\mathbf{u}, \bar{\mathbf{u}})^2 + G(\mathbf{u}, \bar{\mathbf{u}})^c = 0 \quad \forall \bar{\mathbf{u}}^1 \in V^1, \quad \bar{\mathbf{u}}^2 \in V^2, \quad \bar{\mathbf{u}}^c \in V^c \quad (13)$$

where

$$G(\mathbf{u}, \bar{\mathbf{u}})^c = \int_{\Gamma_c} t_n \cdot \bar{g}^n d\Gamma + \int_{\Gamma_c} \mathbf{t}_T \cdot \bar{\mathbf{g}}^T d\Gamma \quad (14)$$

in addition to the constraints $g^n = 0$, $\mathbf{g}^T = 0$.

2.2 Energy approach

In a conservative coupled system, the virtual work functional of Eq. (4) can be alternatively obtained as the minimizer of the total potential energy in the coupled system, which includes the energy stored due to elastic deformations in both domains as well as energy accumulated along the interface. Assuming hyperelastic material behavior in Ω^1, Ω^2 , the energy functional in each domain Ω^i can be expressed as follows

$$\pi_{\Omega^i}(\mathbf{u}^i) = \int_{\Omega^i} [\psi(\mathbf{u}^i) - \mathbf{b}^i \cdot \mathbf{u}^i] d\Omega$$

where $\psi(\mathbf{u}^i)$ is the stored energy density function due to deformations \mathbf{u}^i in domain Ω^i . Interface potential energy is accumulated through the work done by normal and tangential surface tractions and can be expressed as follows

$$\pi^c(\mathbf{u}^1, \mathbf{u}^2) = \int_{\Gamma_c} t_n \cdot g^n d\Gamma + \int_{\Gamma_c} \mathbf{t}_T \cdot \mathbf{g}^T d\Gamma \quad (15)$$

Denoting $\mathbf{u} = [\mathbf{u}^1, \mathbf{u}^2]$ to be the displacement field in the coupled domain, the total potential energy stored in the coupled system can therefore be expressed as follows

$$\pi(\mathbf{u}) = \pi_{\Omega^1}(\mathbf{u}^1) + \pi_{\Omega^2}(\mathbf{u}^2) + \pi^c(\mathbf{u}) \quad (16)$$

Equilibrium of the coupled system corresponds to the stationary point of the modified

energy functional, which is expressed by the directional derivative of the total potential energy functional in the direction of a variational displacement field

$$\begin{aligned} G(\mathbf{u}, \bar{\mathbf{u}}) &= D\pi(\mathbf{u}) \cdot \bar{\mathbf{u}} = D\pi_{\Omega^1}(\mathbf{u}^1) \cdot \bar{\mathbf{u}}^1 + D\pi_{\Omega^2}(\mathbf{u}^2) \cdot \bar{\mathbf{u}}^2 + D\pi^c(\mathbf{u}) \cdot \bar{\mathbf{u}} \\ G(\mathbf{u}, \bar{\mathbf{u}})^1 &= D\pi_{\Omega^1}(\mathbf{u}^1) \cdot \bar{\mathbf{u}}^1 \\ G(\mathbf{u}, \bar{\mathbf{u}})^2 &= D\pi_{\Omega^2}(\mathbf{u}^2) \cdot \bar{\mathbf{u}}^2 \\ G(\mathbf{u}, \bar{\mathbf{u}})^c &= D\pi^c(\mathbf{u}) \cdot \bar{\mathbf{u}} = \int_{\Gamma_c} t_n \cdot \bar{g}^n d\Gamma + \int_{\Gamma_c} \mathbf{t}_T \cdot \bar{\mathbf{g}}^T d\Gamma \end{aligned}$$

The energy approach is only applicable to conservative systems, and thus can be used to enforce normal contact constraints as well as tangential stick conditions. It is, however, the method of choice for the implementation of these constraints using the Lagrange multiplier and penalty approaches.

2.3 Finite element discretization

Defining the finite element partitions $\Omega^1 = \sum_e^1 \Omega_e^1$, $\Omega^2 = \sum_e^2 \Omega_e^2$ in each domain, and adopting the finite element discretizations

$$\bar{\mathbf{u}}^i = \sum_{\alpha} N^{\alpha} \bar{\mathbf{u}}^{\alpha,i}, \quad \mathbf{u}^i = \sum_{\alpha} N^{\alpha} \mathbf{u}^{\alpha,i} \quad \text{in } \Omega_e^i, \quad i = 1, 2$$

within each element, where N^{α} are the interpolation shape functions and $\mathbf{u}^{\alpha,i}$, $\bar{\mathbf{u}}^{\alpha,i}$ are the real and variational nodal displacement vectors at node α in domain i , the discretized finite element form of Eqs. (5)-(7) is obtained as follows

$$G(\mathbf{U}, \bar{\mathbf{U}})^i = [\mathbf{R}^i - \mathbf{Q}^i] \cdot \bar{\mathbf{U}}^i, \quad i = 1, 2. \quad (15)$$

In this equation $\mathbf{U} = [\mathbf{U}^1, \mathbf{U}^2]$ and $\bar{\mathbf{U}} = [\bar{\mathbf{U}}^1, \bar{\mathbf{U}}^2]$ are the real and virtual nodal displacement vectors in the coupled system, and \mathbf{R}^i , \mathbf{Q}^i are the equivalent external and internal nodal load vectors in domain i , respectively.

$$\begin{aligned} \mathbf{R}^i &= \prod_{\alpha}^{e,i} \left[\int_{\Omega_e^i} N^{\alpha} \mathbf{b}^i d\Omega + \int_{\Gamma_e^i} N^{\alpha} \mathbf{t}^i d\Gamma \right], \\ \mathbf{Q}^i &= \prod_{\alpha}^{e,i} \left[\int_{\Omega_e^i} \mathbf{B}^T(N^{\alpha}) \cdot \boldsymbol{\sigma}^i d\Omega \right], \end{aligned} \quad (16)$$

where $\prod_{\alpha}^{e,i}$ is the assembly operator for domain i and $\nabla \bar{\mathbf{u}}^2 = \mathbf{B}(N^{\alpha}) \bar{\mathbf{u}}^{\alpha,i}$.

2.4 Enforcing normal and tangential stick constraints

Methods for enforcing contact constraints differ in their definition of the contact energy $\pi^c(\mathbf{u})$ and interface stress fields. In the penalty method, the contact energy is the norm of the gap function penalized by a large penalty parameter. The Lagrange multiplier approach introduces a field of Lagrange multipliers along the interface to enforce the non-overlap condition at contact locations. In a discretized finite element mesh, discrete Lagrange multipliers are applied at a number of slave nodes on the contact interface, leading to the following contact energy functional for all contact nodes N at the interface

$$\pi^c(\mathbf{U}, \boldsymbol{\lambda}, \boldsymbol{\lambda}_T) = \sum_{i=1}^N \lambda_i g_i^n + \sum_{i=1}^N \boldsymbol{\lambda}_{T_i} \cdot \mathbf{g}_i^T \quad (17)$$

Eq. (17) represents the discretized contact energy functional along the interface. The Lagrange multipliers λ and λ_T can be interpreted to be the equivalent nodal forces for normal contact pressure and tangential tractions at the slave contact points, respectively. Taking the directional derivative of the potential energy functional with respect to $\mathbf{U}, \lambda, \lambda_T$, the discretized weighted residual functional for the coupled system is

$$\begin{aligned}
 G(\mathbf{U}, \bar{\mathbf{U}})^c &= D\pi^c(\mathbf{U}, \lambda, \lambda_T) \cdot \bar{\mathbf{u}} = \sum_{i=1}^N \lambda_i \bar{g}_i^n + \sum_{i=1}^N \lambda_{T_i} \cdot \bar{\mathbf{g}}_i^T = G(\mathbf{U}, \bar{\mathbf{U}})_n^c + G(\mathbf{U}, \bar{\mathbf{U}})_T^c \\
 D\pi^c(\mathbf{U}, \lambda, \lambda_T) \cdot \lambda_i &= g_i^n \\
 D\pi^c(\mathbf{U}, \lambda, \lambda_T) \cdot \lambda_{T_i} &= \mathbf{g}_i^T
 \end{aligned}$$

In the above equations we assumed that interface compatibility applies are all times. In contact problems, unilateral constraints are used to allow the two bodies to separate from each other. Furthermore, lateral conditions are typically governed by the Coulomb frictional law that allows for tangential sliding once a limit tangential traction value is reached. In the following sections we describe how the above equations can be modified to account for unilateral constraints in the direction normal to the interface as well as stick/slip variations in the tangential direction.

2.4.1 Unilateral normal contact constraints

The simplest and earliest method for enforcing normal contact conditions is the Node-to-Surface approach illustrated in Fig. 3 (Wriggers 2006). The Node-To-Surface (NTS) contact constraint measures the normal gap or oriented distance between a “slave” node on one side of the interface and its projection on the opposing “master” surface. The bodies on either side of the interface are free to move apart or come in contact with each other and the sign of the gap function is used to distinguish between the positioning of one body with respect to the other, as shown in Fig. 4.

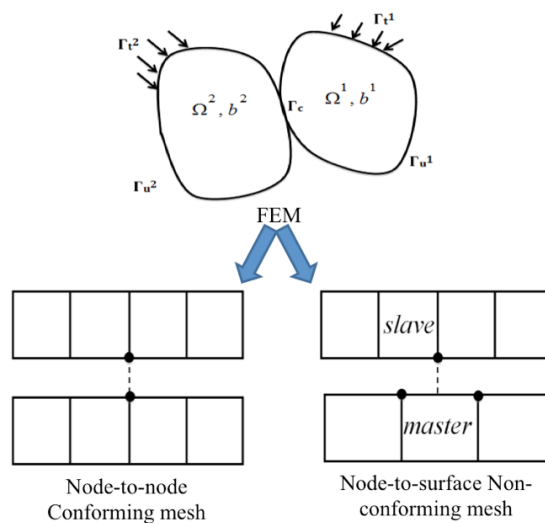


Fig. 3 FEM Interface Discretization

For the displacement field to represent an admissible kinematic state, there could be no overlap penetration or mass inter-penetration between the two bodies. This condition is typically reflected through the unilateral contact constraint function

$$g^n = (\mathbf{x} - \mathbf{x}^P) \cdot \mathbf{n} \geq 0 \text{ for all } \mathbf{x} \in \Gamma_c \tag{18}$$

In this equation g^n is the normal component of the gap between the two bodies, defined by the closest projection \mathbf{x}^P of a point \mathbf{x} on the boundary of one body (slave surface) to the surface of the other body (master surface), and \mathbf{n} is the normal vector to the master surface at the projection point. The closest point projection \mathbf{x}^P of a slave node \mathbf{x} on the master surface is the minimizer of the distance $\mathbf{x} - \mathbf{x}^P$.

With the isoparametric interpolation of the spatial variables in the master element $\mathbf{x}^P = \sum_{\alpha} N^{\alpha}(\boldsymbol{\xi}^P)\mathbf{x}^{\alpha}$, the minimization problem reduces to finding the coordinates $\boldsymbol{\xi}^P$ that correspond to the closest point projection \mathbf{x}^P of \mathbf{x} on the master element surface.

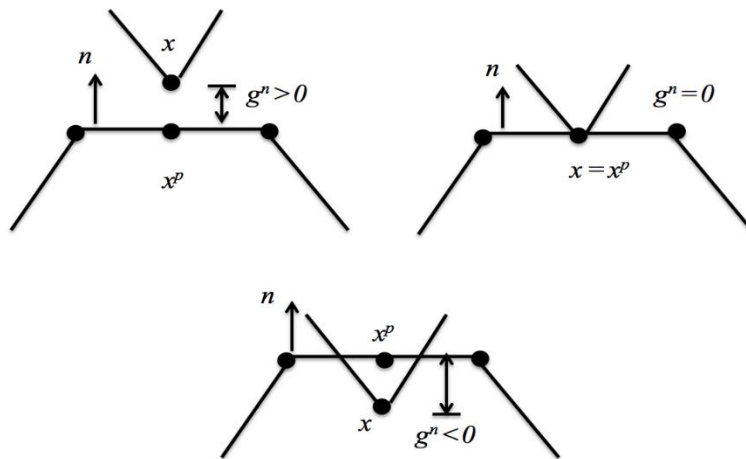


Fig. 4 Gap Function

The normal gap function is enforced with a normal pressure field at the interface (λ), and governed by the contact Kuhn-Tucker conditions summarized in Fig. 5.

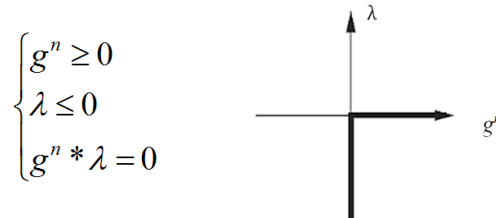


Fig. 5 Kuhn-Tucker Conditions (Left) and Contact Forces vs. Normal Gap (Right)

We implement an active set strategy and include the constraints at slave nodes one by one starting with the most violated. Thus, the discretized virtual work for normal tractions on the

interface is given by

$$G(\mathbf{U}, \bar{\mathbf{U}})_n^c = \sum_{i=1}^N \lambda_i \bar{g}_i^n \quad (19)$$

$$\begin{aligned} \lambda_i &\leq 0 \\ \bar{g}_i^n &\geq 0 \end{aligned} \quad \forall i \in \text{active set.}$$

2.4.2 Coulomb frictional contact formulation

Frictional contact behavior governs the relationship between tangential interface tractions \mathbf{t}_T and the relative tangential motion between two contacting points at the contact interface between the two bodies, \mathbf{g}^T . We implement the widely used Coulomb constitutive model in the present formulation of the frictional contact. According to this model, points along the contact interface can be in either a stick or slip state. The stick state occurs when the norm of the tangential component of the interface traction vector, \mathbf{t}_T , is less than the frictional resistance of the interface, defined to be equal to the normal contact force multiplied by the friction coefficient μ . In this case, no relative tangential displacement occurs. Slip happens when the applied force reaches the maximum frictional resistance and causes a relative tangential displacement.

The stick/slip criterion of the Coulomb model can be expressed as an inequality slip function that relates \mathbf{t}_T and the normal component of the traction t_n through the friction coefficient μ as

$$f(\mathbf{t}_T, t_n) = \|\mathbf{t}_T\| - \mu t_n \leq 0 \quad (20)$$

The stick state occurs when $\|\mathbf{t}_T\| \leq \mu t_n$, in which case no tangential relative motion occurs $\dot{\mathbf{g}}^T = \mathbf{0}$, while the slip state occurs when $\|\mathbf{t}_T\| > \mu t_n$ leading to a non-zero slip rate $\|\dot{\mathbf{g}}^T\| > 0$ in the direction \mathbf{r} , tangent to the contact surface. This leads to the Kuhn-Tucker conditions for frictional contact

$$\begin{aligned} \dot{\mathbf{g}}^T &= \gamma \mathbf{r}, \quad \gamma > 0 \\ f &\leq 0 \\ \gamma f &= 0 \end{aligned}$$

These constraints are implemented at all contact locations i , and included in the tangential part of the interface virtual work in the following form

$$G(\mathbf{u}, \bar{\mathbf{u}})_T^c = \sum_{i=1}^N \lambda_{T_i} \cdot \bar{\mathbf{g}}_i^T, \quad \mathbf{g}_i^T = \mathbf{0} \quad \text{at stick locations} \quad (21)$$

$$G(\mathbf{u}, \bar{\mathbf{u}})_T^c = \sum_{i=1}^N \mathbf{t}_T \cdot \bar{\mathbf{g}}_i^T, \quad \|\mathbf{t}_T\| = \mu t_n \quad \|\mathbf{g}_i^T\| > \mathbf{0} \quad \text{at slip locations} \quad (22)$$

In the case of stick, the work done by the tangential forces vanishes, and therefore, the formulation remains conservative. When slip is detected, the negative work done by the tangential forces leads to a dissipation of energy. The stick-slip transition is handled using the augmented Lagrangian approach. The relationship between the tangential traction and relative slip can be represented as

$$\mathbf{t}_T = -\epsilon_T \mathbf{g}^T$$

where ϵ_T is interpreted as the tangential interface stiffness, and is the penalty parameter used to enforce the stick condition $\mathbf{g}^T = \mathbf{0}$. This relationship can also be defined using a friction potential φ such that $\mathbf{t}_T = \partial\varphi/\partial\mathbf{g}^T$, where more elaborate interface models that include adhesion and/or damage can be incorporated. Potential-based methods, such as the bi-potential approach (De Saxce and Feng 1998) have been used successfully in the presence of large deformations and dynamic effects (Terfaya *et al.* 2015). Penalty-based methods can be sensitive to the choice of the interface stiffness parameter ϵ_T .

The distinction between stick/slip conditions at each contact location i is required to properly account for the tangential work done on the interface. In the case of stick, a constraint has to be placed on lateral displacements to prevent sliding $\mathbf{g}_i^T = \mathbf{0}$, whereas in the case of slip, the tangential displacements are released and a tangential force $\|\mathbf{t}_T\| = \mu t_n$ is applied instead. For each load increment an assumption of stick /slip condition is made at each contact point. This assumption is revisited after completing the solution of the nonlinear problem, typically using the Newton method. If the initial assumption is found to be no longer correct, the Newton solution is repeated under revised assumptions. In a large finite element mesh where the contact state at a number of interface nodes could potentially change between stick and slip, this approach in enforcing frictional constraints has been found to be the source of algorithmic instability (Gu *et al.* 2009).

The dilemma in deciding the stick/slip conditions at contact nodes recalls a similar issue in computing stresses in the theory of rate-independent plasticity. Much like the frictional case, the stresses in plasticity are bound by a “yield” function upon which the material starts accruing irreversible plastic flow that occurs normal to the yield surface and does not correspond to an increase in stress. For frictional contact, tangential slip can be thought of as the equivalent of plastic strain, i.e. an irreversible state of deformation not associated with an increase in tangential stress/force beyond a limit dictated by the yield function of the Coulomb model (Eq. (20)). Furthermore, the stresses and deformations beyond “yielding” in frictional contact are governed by a similar set of Kuhn-Tucker conditions.

Therefore, an alternative approach to enforcing frictional contact conditions is to compute the tangential tractions through an inner-subroutine, activated at the contact point, that releases the flow of slip displacement in the case where the yield potential, in this case called the slip criterion, is exceeded. The tangential relative displacements are decomposed into a reversible or stick component, that correspond to a stick state, and an irreversible slip component that accrues when the yield potential is exceeded. Tangential tractions are computed through a return-mapping algorithm not to exceed the Coulomb limit with slip variables as history-depended internal variables, calculated and stored locally at contact locations. This approach is algorithmically superior since it does not require the repetition of the Newton solution anytime the slip criterion is violated and slip is activated at a given contact location, thereby substantially reducing computational cost and potential instability, as shown in Fig. 6.

This method was introduced in the early work of (Ibrahimbegovic and Wilson 1991), and has been adopted by numerous researchers in the frictional contact community (Laursen and Simo 1993b, Sheng *et al.* 2006, Masud *et al.* 2012) although its application has been restricted to the case of small-deformation linear problems for reasons that will become obvious in the discussion below. Due to the issues associated with penalty-based methods and mixed formulations, and given the effectiveness of the stick-slip decomposition approach in handling the transition between stick and slip states, the aim of this work is to propose a new methodology for applying the stick-slip decomposition approach to large-deformation problems.

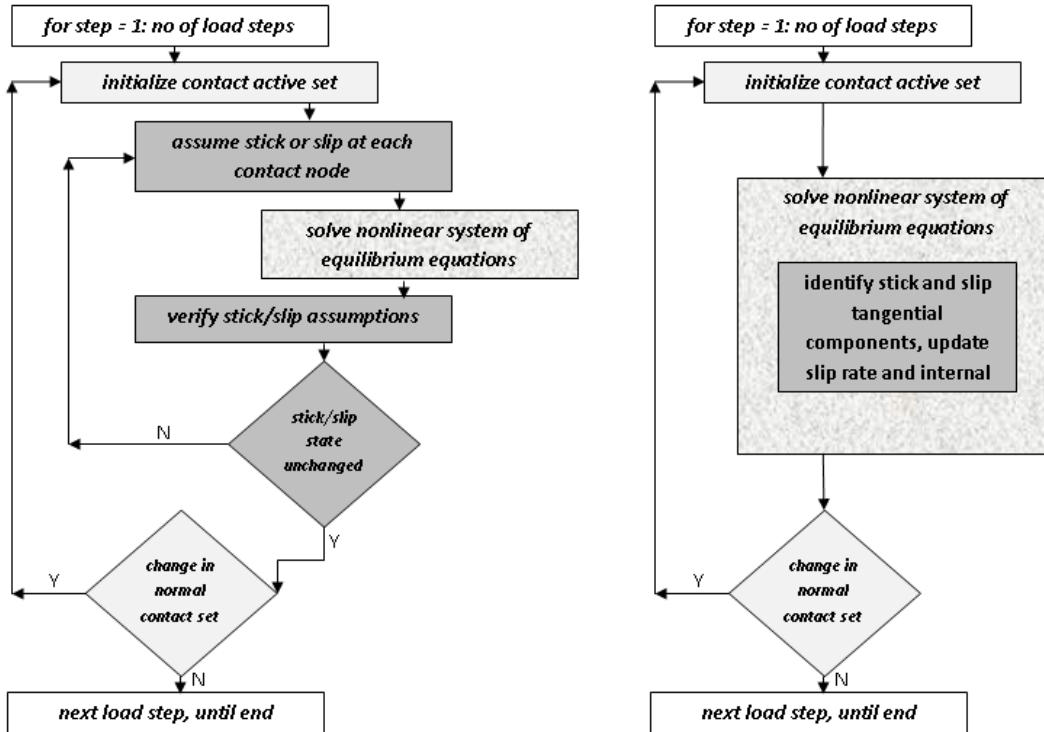


Fig. 6 Standard friction algorithm (left) vs. The local stick-slip decomposition approach (right)

We propose a new formulation for hyperelastic large-deformation frictional contact based on the stick/slip decomposition method. This approach handles the numerical issues encountered when modeling the stick/slip Coulomb frictional contact models. Our approach handles the stick/slip condition in an inner loop inside the Newton solver without the need of a repeated solution.

We start our formulation for the case of small deformations, which has been done also in other studies in literature, in order to illustrate the challenge in extending this approach to the large-deformation frictional contact problem.

2.5 The stick-slip decomposition approach for small-deformation frictional contact

Let us assume that the total tangential displacement is decomposed into two components: a reversible “elastic” component \mathbf{u}_T^e and an irreversible “plastic” slip \mathbf{u}_T^p such as: $\mathbf{u}_T = \mathbf{u}_T^e + \mathbf{u}_T^p$ (Laursen and Simo 1993b). The total displacement therefore on the slave side of the interface

$$\mathbf{u} = u_n \mathbf{n} + \mathbf{u}_T^e + \mathbf{u}_T^p \tag{23}$$

An estimate of interface tractions can be calculated from Eq. (23) based on the element constitutive behavior and finite element discretization. However, since the formulation of the equations of motion is done in the discretized finite element space, and given that contact constraints are enforced strictly at the slave nodes, it is more convenient to write the relationship between interfacial force and kinematic fields in terms of equivalent nodal internal

forces \mathbf{Q} and nodal displacements \mathbf{U} . Adopting a similar decomposition for the nodal displacement vector at the contact slave node, we can write the equation for the nodal internal force as it is computed from the total nodal displacements as follows

$$\mathbf{Q}(\mathbf{U}) = \mathbf{Q}(U_n \mathbf{n} + \mathbf{U}_T^e + \mathbf{U}_T^p) = \mathbf{K}(U_n \mathbf{n} + \mathbf{U}_T^e + \mathbf{U}_T^p) \quad (24)$$

where \mathbf{K} is the element stiffness matrix. Assuming linear elastic material behavior and small deformations, Eq. (24) can be re-written as

$$\mathbf{Q}(\mathbf{U}) = \mathbf{K}(U_n \mathbf{n} + \mathbf{U}_T^e) + \mathbf{K}(\mathbf{U}_T^p) \quad (25)$$

A key benefit to Eq. (25) is that it provides a natural means for computing interface stiffness using element stiffness matrices, as opposed to relying on artificial user-defined penalty parameters. The first part of Eq. (25) represents the force associated with the normal component of the displacement as well as the reversible or “stick” component of the tangential displacement on the interface. The second part of the force vector corresponds to the change in force due to the occurrence of tangential slip. It follows that the reversible component of the interface nodal force is expressed as

$$\mathbf{Q} = \mathbf{Q}^e = \mathbf{K}(U_n \mathbf{n} + \mathbf{U}_T^e) = \mathbf{K}(\mathbf{U} - \mathbf{U}_T^p) \quad (26)$$

Note that this equation is written for the total interface nodal force. The normal component of \mathbf{Q}^e represents the normal interface force needed to enforce the normal inter-penetrability constraints, while the tangential component of \mathbf{Q}^e is responsible for enforcing tangential stick conditions $g_T(\mathbf{U}_T^e) = \mathbf{0}$. This formulation differs from other implementations of the stick-slip decomposition method in which separate constitutive equations are used for the normal and tangential components of interface forces. These implementations are often based on the penalty approach for enforcing the normal (interpenetration) and tangential (stick) conditions, where the respective penalty parameters represent interface stiffness in the normal and tangential directions. It is not possible, however, to enforce perfect stick condition with the penalty formulation, and the corresponding penalty stiffness is an artificial estimate of interface resistance to tangential sliding. The present approach estimates tangential motion resistance directly from the finite element estimate of stiffness associated with elastic deformations on the interface.

Remark: Note that the kinematic variable in Eq. (26) is the absolute tangential slip displacement at the slave node \mathbf{U}_T and not tangential gap function $\mathbf{g}^T = \mathbf{U}_T - \mathbf{u}_T^M$, where \mathbf{u}_T^M is the tangential displacement on the master side of the interface. This is the result of using the element stiffness relationship, as pointed out in Eq. (25). However, since $\mathbf{U}_T, \mathbf{u}_T^M$ are independent variables, Eq. (26) can be re-written in terms of \mathbf{g}^T when necessary and without substantial impact on the formulation, as follows

$$\mathbf{g}^T = \mathbf{U}_T - \mathbf{u}_T^M = [\mathbf{U}_T^e + \mathbf{U}_T^p] - [\mathbf{u}_T^{M,e} + \mathbf{u}_T^{M,p}] = \mathbf{g}_T^e + \mathbf{g}_T^p$$

where $\mathbf{g}_T^e = \mathbf{U}_T^e - \mathbf{u}_T^{M,e} = \mathbf{0}$ is the “stick” tangential gap, which is enforced to be zero, and $\mathbf{g}_T^p = \mathbf{U}_T^p - \mathbf{u}_T^{M,p}$ is the relative slip tangential displacement. It follows, therefore, that

$$\begin{aligned} \mathbf{g}^T &= \mathbf{g}_T^p \\ \mathbf{U}_T &= \mathbf{g}^T + \mathbf{u}_T^M = \mathbf{g}_T^p + \mathbf{u}_T^M \end{aligned}$$

Substituting into Eq. (26), we find an alternative form of the modified stiffness equation for the

internal force at the slave node in terms of the relative slip displacement as

$$\mathbf{Q} = \mathbf{K}(\mathbf{U} - \mathbf{U}_T) = \mathbf{K}([\mathbf{U} - \mathbf{u}_T^M] - \mathbf{g}_T^p) \quad (27)$$

Since $g^n = 0$ at the contact location, $\mathbf{U} - \mathbf{u}_T^M$ represents the relative tangential motion between the two points across the interface.

According to Coulomb friction law, the tangential interface force component cannot exceed the limit of μt_n , where t_n is the normal nodal pressure and μ is the surface frictional coefficient. The Coulomb friction law therefore follows the slip criterion

$$f = \|\mathbf{Q}_T\| - \mu Q_n \leq 0 \quad (28)$$

Let $\mathbf{P} = [\mathbf{I} - \mathbf{n} \otimes \mathbf{n}]$ the projection tensor on the contact surface with normal \mathbf{n} . It follows that the norm of the tangential force vector can be computed as

$$\mathbf{Q}_T = \mathbf{P}\mathbf{Q}, \quad \|\mathbf{Q}_T\| = \sqrt{\mathbf{P}\mathbf{Q} \cdot \mathbf{P}\mathbf{Q}} = \sqrt{\mathbf{Q} \cdot \mathbf{P}^2\mathbf{Q}} = \sqrt{\mathbf{Q} \cdot \mathbf{P}\mathbf{Q}} \quad (29)$$

where $\mathbf{P}^2 = \mathbf{P}\mathbf{P} = \mathbf{P}^T\mathbf{P} = \mathbf{P}$. Recognizing that $Q_n = \mathbf{Q} \cdot \mathbf{n}$ equation can be re-written as

$$f = \sqrt{\mathbf{Q} \cdot \mathbf{P}\mathbf{Q}} - \mu \mathbf{Q} \cdot \mathbf{n} \leq 0 \quad (30)$$

The value of $f \leq 0$ corresponds to a stick state; while $f > 0$ is an inadmissible state that indicates the onset of tangential “plastic” slip. When plastic slip is initiated a return mapping algorithm is activated to return the tangential forces to the slip surface. We assume that the “flow” of irreversible slip displacement occurs tangent to the contact interface, therefore resulting in non-associative flow rule with return mapping \mathbf{r} such that

$$\dot{\mathbf{U}}_T^p = \gamma \mathbf{r} \quad (31)$$

$$\mathbf{r} = \frac{\mathbf{P}\mathbf{Q}}{\|\mathbf{P}\mathbf{Q}\|} = \frac{\mathbf{P}\mathbf{Q}}{\sqrt{\mathbf{Q} \cdot \mathbf{P}\mathbf{Q}}} \quad (32)$$

In Eq. (31) γ is the rate-independent consistency parameter that enforces the persistency condition. i.e., $f = 0$. Eq. (31) defines the direction of slip flow as tangent to the contact surface. It has to be noted that this direction does not correspond to an associative flow rule as $\mathbf{r} \neq \partial f / \partial \mathbf{Q}$.

The governing equations for the Coulomb frictional problem can therefore be summarized as follows

$$\begin{aligned} \mathbf{Q} &= \mathbf{K}(U_n \mathbf{n} + \mathbf{U}_T^c) = \mathbf{K}(\mathbf{U} - \mathbf{U}_T^p) \\ f &= \sqrt{\mathbf{Q} \cdot \mathbf{P}\mathbf{Q}} - \mu \mathbf{Q} \cdot \mathbf{n} \\ \dot{\mathbf{U}}_T^p &= \gamma \mathbf{r}, \quad \mathbf{r} = \mathbf{P}\mathbf{Q} / \sqrt{\mathbf{Q} \cdot \mathbf{P}\mathbf{Q}} \\ \gamma &> 0, \quad f \leq 0, \quad \gamma f = 0 \end{aligned} \quad (32)$$

along with the persistency condition $\gamma \dot{f} = 0$

In a quasi-static time-stepping finite element solution, Eqs. (32) are discretized in time using the Backward Euler approach. Assuming \mathbf{Q}_n , \mathbf{U}_T^p and \mathbf{U}_n are the nodal forces, tangential slip and total displacement at a contact point at step n , the discretized governing equations for the Coulomb friction model at step $n + 1$ are calculated as follows: First a trial state for interface forces is calculated using current displacement estimates

$$\begin{aligned} \mathbf{Q}_{n+1}^{trial} &= \mathbf{K}(\mathbf{U}_{n+1} - \mathbf{U}_{T_n}^p) \\ f_{n+1}^{trial} &= \sqrt{\mathbf{Q}_{n+1}^{trial} \cdot \mathbf{P}\mathbf{Q}_{n+1}^{trial}} - \mu \mathbf{Q}_{n+1}^{trial} \cdot \mathbf{n} \end{aligned} \quad (33)$$

If $f_{n+1}^{trial} > 0$, slip is activated and the following return-mapping algorithm is applied

$$\begin{aligned} \mathbf{Q}_{n+1}^{trial} &= \mathbf{K}(\mathbf{U}_{n+1} - \mathbf{U}_{T_n}^p) \\ \mathbf{U}_{T_{n+1}}^p &= \mathbf{U}_{T_n}^p + \bar{\gamma} \mathbf{r}_{n+1} \\ \mathbf{r}_{n+1} &= \mathbf{P}\mathbf{Q}_{n+1} / \sqrt{\mathbf{Q}_{n+1} \cdot \mathbf{P}\mathbf{Q}_{n+1}} \\ \bar{\gamma} &= \gamma \Delta t \\ \mathbf{Q}_{n+1} &= \mathbf{Q}_{n+1}^{trial} - \bar{\gamma} \mathbf{K}\mathbf{r}_{n+1} \\ f_{n+1} &= \sqrt{\mathbf{Q}_{n+1} \cdot \mathbf{P}\mathbf{Q}_{n+1}} - \mu \mathbf{Q}_{n+1} \cdot \mathbf{n} = 0 \end{aligned} \quad (34)$$

Eqs. (34) are used to calculate $\bar{\gamma}$ and update the slip displacement and nodal forces at step $n + 1$.

Consistent Tangent:

The consistent tangent matrix \mathbf{T} is computed by evaluating the partial derivative of the force vector \mathbf{Q}_{n+1} with respect to the displacement \mathbf{u}_{n+1} as follows

$$\mathbf{T}_{n+1} = \frac{\partial \mathbf{Q}_{n+1}}{\partial \mathbf{U}_{n+1}} = \frac{\partial \mathbf{Q}_{n+1}^{trial}}{\partial \mathbf{U}_{n+1}} - \bar{\gamma} \mathbf{K} \frac{\partial \mathbf{r}_{n+1}}{\partial \mathbf{U}_{n+1}} - \mathbf{K} \mathbf{r}_{n+1} \otimes \frac{\partial \bar{\gamma}}{\partial \mathbf{U}_{n+1}} \quad (35)$$

In this equation

$$\frac{\partial \mathbf{Q}_{n+1}^{trial}}{\partial \mathbf{U}_{n+1}} = \mathbf{K} \quad (36)$$

$$\frac{\partial \mathbf{r}_{n+1}}{\partial \mathbf{U}_{n+1}} = \frac{\partial \mathbf{r}_{n+1}}{\partial \mathbf{Q}_{n+1}} \frac{\partial \mathbf{Q}_{n+1}}{\partial \mathbf{U}_{n+1}} = \mathbf{S}_{n+1} \mathbf{T}_{n+1} \quad (37)$$

$$\mathbf{S}_{n+1} = \frac{\partial \mathbf{r}_{n+1}}{\partial \mathbf{Q}_{n+1}} = \frac{[\mathbf{P} - \mathbf{r}_{n+1} \otimes \mathbf{r}_{n+1}]}{\sqrt{\mathbf{Q}_{n+1} \cdot \mathbf{P}\mathbf{Q}_{n+1}}} \quad (38)$$

where \mathbf{K} is the elastic stiffness matrix and \mathbf{S} is a projection matrix on the friction potential surface. Substituting Eqs. (36)-(38) in Eq. (35), the equation for the consistent tangent can be simplified as follows

$$\mathbf{T}_{n+1} = \frac{\partial \mathbf{Q}_{n+1}}{\partial \mathbf{U}_{n+1}} = \mathbf{K} - \bar{\gamma} \mathbf{K} \mathbf{S}_{n+1} \mathbf{T}_{n+1} - \mathbf{K} \mathbf{r}_{n+1} \otimes \frac{\partial \bar{\gamma}}{\partial \mathbf{U}_{n+1}} \quad (39)$$

$$\mathbf{K} [\mathbf{K}^{-1} + \bar{\gamma} \mathbf{S}_{n+1}] \mathbf{T}_{n+1} = \mathbf{K} - \mathbf{K} \mathbf{r}_{n+1} \otimes \frac{\partial \bar{\gamma}}{\partial \mathbf{U}_{n+1}} \quad (40)$$

$$\mathbf{T}_{n+1} = \mathbf{A}^{-1} - \mathbf{A}^{-1} \mathbf{r}_{n+1} \otimes \frac{\partial \bar{\gamma}}{\partial \mathbf{U}_{n+1}} \quad (41)$$

where $\mathbf{A} = [\mathbf{K}^{-1} + \bar{\gamma} \mathbf{S}_{n+1}]$ is the modified flexibility tensor. In order to compute the derivative of $\bar{\gamma}$ with respect to the displacement \mathbf{U}_{n+1} we note that, by taking the derivative of the slip function with respect to \mathbf{u}_{n+1} we obtain the orthogonality condition

$$\frac{\partial f_{n+1}}{\partial \mathbf{U}_{n+1}} = \frac{\partial f_{n+1}}{\partial \mathbf{Q}_{n+1}} \frac{\partial \mathbf{Q}_{n+1}}{\partial \mathbf{U}_{n+1}} = \mathbf{h}_{n+1}^T \mathbf{T}_{n+1} = 0 \quad (42)$$

where

$$\mathbf{h}_{n+1} = \frac{\partial f_{n+1}}{\partial \mathbf{Q}_{n+1}} = \frac{\mathbf{PQ}_{n+1}}{\sqrt{\mathbf{Q}_{n+1} \cdot \mathbf{PQ}_{n+1}}} - \mu \mathbf{n} \quad (43)$$

is the normal to the Coulomb surface. Pre-multiplying Eq. (35) by \mathbf{h}_{n+1}^T and substituting Eqs. (36)-(38), we find

$$\mathbf{h}_{n+1}^T \mathbf{T}_{n+1} = 0 = \mathbf{h}_{n+1}^T \mathbf{A}^{-1} - \mathbf{h}_{n+1}^T \mathbf{A}^{-1} \mathbf{r}_{n+1} \frac{\partial \bar{\gamma}}{\partial \mathbf{U}_{n+1}}$$

which, in combination with Eq. (39) leads to

$$\frac{\partial \bar{\gamma}}{\partial \mathbf{U}_{n+1}} = \frac{1}{\mathbf{h}_{n+1}^T \mathbf{A}^{-1} \mathbf{r}_{n+1}} \mathbf{h}_{n+1}^T \mathbf{A}^{-1} \quad (44)$$

Substituting Eqs. (36), (37), (44) into Eq. (35), the expression for the consistent tangent reduced to

$$\begin{aligned} \mathbf{T}_{n+1} &= \mathbf{A}^{-1} - \frac{1}{\mathbf{h}_{n+1}^T \mathbf{A}^{-1} \mathbf{r}_{n+1}} \mathbf{A}^{-1} \mathbf{r}_{n+1} \otimes \mathbf{A}^{-1} \mathbf{h}_{n+1} \\ &= \mathbf{A}^{-1} - \mathbf{v}_{n+1} \otimes \mathbf{w}_{n+1} \end{aligned} \quad (45)$$

where

$$\mathbf{v}_{n+1} = \frac{\mathbf{A}^{-1} \mathbf{r}_{n+1}}{\sqrt{\mathbf{h}_{n+1}^T \mathbf{A}^{-1} \mathbf{r}_{n+1}}} \quad (46)$$

$$\mathbf{w}_{n+1} = \frac{\mathbf{A}^{-1} \mathbf{h}_{n+1}}{\sqrt{\mathbf{h}_{n+1}^T \mathbf{A}^{-1} \mathbf{r}_{n+1}}} \quad (47)$$

It is worth noting that, without additional consideration, this formulation does not guarantee a perfect stick condition. In other words, there could exist a non-zero lateral displacement that would not cause the violation of the slip criterion. This issue, however, can be remedied by enforcing an additional constraint on the tangential component of the “stick” displacement to be zero such that the virtual work functional for the system is expressed as

$$G(\mathbf{u}, \bar{\mathbf{u}}) = G(\mathbf{U}, \bar{\mathbf{U}})^1 + G(\mathbf{U}, \bar{\mathbf{U}})^2 + G(\mathbf{U}, \bar{\mathbf{U}})^c = 0$$

$$G(\mathbf{U}, \bar{\mathbf{U}})^c = \sum_{i=1}^N \lambda_i \bar{g}_i^n + \sum_{i=1}^N \lambda_{T_i} \cdot \bar{\mathbf{g}}_i^T \quad (48)$$

in addition to the lateral stick and normal contact conditions

$$\mathbf{g}_i^T = \mathbf{0} \quad (49)$$

$$\lambda_i \leq 0, \bar{g}_i^n = 0 \tag{50}$$

2.6 Large-deformation frictional contact

Extending the above to the case of large-deformation problems is hindered by the fact that Eq. (26) no longer holds when the traction is a nonlinear function of the displacements. In other words, an additive decomposition of the displacement field does not translate into a similar result for the traction field. Therefore, the return-mapping algorithm, as described above cannot be implemented.

A direct approach to remedy this problem is to implement a procedure similar to large-deformation computational plasticity theory by following the idea of a multiplicative decomposition of the deformation gradient into elastic and plastic parts as: $\mathbf{F} = \mathbf{F}^e \mathbf{F}^p$ (Simo *et al.* 1985). For frictional contact, the elastic and plastic parts of \mathbf{F} correspond to the stick and slip response modes, respectively.

Recalling that $\mathbf{F} = \frac{d\mathbf{x}}{d\mathbf{X}}$, where \mathbf{x} and \mathbf{X} are the spatial and material variables, respectively, we can assume that it is possible to find a stress-free plastic state $\tilde{\mathbf{x}}$ such that $\mathbf{F}^p = \frac{d\tilde{\mathbf{x}}}{d\mathbf{X}}$ and $\mathbf{F}^e = \frac{d\mathbf{x}}{d\tilde{\mathbf{x}}}$, as shown in Fig. 7. The right Cauchy-Green strain tensor $\mathbf{C} = \mathbf{F}^T \mathbf{F}$ can be derived from both the elastic $\mathbf{C}^e = \mathbf{F}^{eT} \mathbf{F}^e$ and plastic $\mathbf{C}^p = \mathbf{F}^{pT} \mathbf{F}^p$ components of \mathbf{F} . The “reversible” left Cauchy-Green strain tensor \mathbf{b}^e is given as $\mathbf{b}^e = \mathbf{F}^e \mathbf{F}^{eT} = \mathbf{F} \mathbf{F}^{p-1} \mathbf{F}^{p-T} \mathbf{F}^T = \mathbf{F} \mathbf{C}^{p-1} \mathbf{F}^T$.

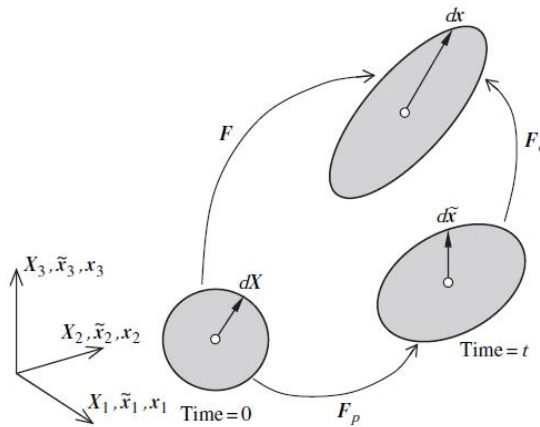


Fig. 7 Multiplicative Decomposition of the Deformation Gradient (Bonet and Woods 2008)

We write the above fields in terms of the principal directions since they are invariant with arbitrary rigid-body rotation. Accordingly, the left reversible Cauchy-Green strain tensor is represented by the principal elastic stretches λ_α^e , and the corresponding principle directions \mathbf{n}_α as

$$\mathbf{b}^e = \sum_{\alpha=1}^3 (\lambda_\alpha^e)^2 \mathbf{n}_\alpha \otimes \mathbf{n}_\alpha \tag{51}$$

The return mapping procedure is thus strain driven. The global system of equations sends a strain update to a material point in the form of an estimated deformation gradient \mathbf{F}_{n+1} . Using the previous converged solution and the current assumed trial solution, a trial value of the reversible deformation tensor can be found

$$\mathbf{b}_{n+1}^{e,trial} = \mathbf{F}_{n+1} \mathbf{C}_n^{p^{-1}} \mathbf{F}_{n+1}^T \quad (52)$$

The trial stretches in the principal directions can then be found by solving for the Eigenvalues and Eigenvectors of $\mathbf{b}_{n+1}^{e,trial}$

$$\mathbf{b}_{n+1}^{e,trial} = \sum_{\alpha=1}^3 (\lambda_{\alpha}^{e,trial})^2 \mathbf{n}_{\alpha}^{trial} \otimes \mathbf{n}_{\alpha}^{trial} \quad (53)$$

A trial state of stress is calculated based on $\mathbf{b}_{n+1}^{e,trial}$, and if the yield function is exceeded, the principal stretches are updated using a return mapping algorithm in directions $\mathbf{n}_{\alpha}^{n+1}$

$$\ln \lambda_{\alpha}^{e,n+1} = \ln \lambda_{\alpha}^{e,trial} - \bar{\gamma} \nu_{\alpha}^{n+1} \quad (54)$$

$$\nu_{\alpha}^{n+1} = \partial f^{n+1} / \partial \tau_{\alpha\alpha} \quad (55)$$

where $\tau_{\alpha\alpha}$ is the principal stress in the direction α . The plastic deformation tensor is then obtained from an updated strain tensor as follows

$$\mathbf{b}_{n+1}^e = \sum_{\alpha=1}^3 (\lambda_{\alpha}^{e,n+1})^2 \mathbf{n}_{\alpha}^{trial} \otimes \mathbf{n}_{\alpha}^{trial} \quad (56)$$

$$\mathbf{C}_{n+1}^{p^{-1}} = \mathbf{F}_{n+1}^{-1} \mathbf{b}_{n+1}^e \mathbf{F}_{n+1}^{-T} \quad (57)$$

The fact that the plastic deformation is computed through the strain tensor $\mathbf{C}^{p^{-1}}$, however, limits the application of this approach for frictional contact since it would not be possible to enforce perfect stick conditions. This is due to the fact that the plastic displacement \mathbf{u}_T^p required to enforce these conditions is not a variable in this formulation.

3. Proposed stick-slip decomposition for large-deformation frictional contact

We propose an approach for implanting the stick-slip decomposition method while preserving the additive split of the displacement field: $\mathbf{u}_T = \mathbf{u}_T^e + \mathbf{u}_T^p$ in order to enable the enforcement of perfect stick conditions. To circumvent the fact that this decomposition does not correspond to an additive split of the traction field, we propose using a linearized form of the traction vector, based on a Taylor series expansion around the elastic (stick) displacement as follows:

Let \mathbf{Q} be the nodal interface force at a given contact location. In a hyper-elastic material under large deformations, the force is a nonlinear function of the total displacement vector

$$\mathbf{Q}(\mathbf{U}) = \mathbf{Q}(U_n \mathbf{n} + \mathbf{U}_T^e + \mathbf{U}_T^p) \quad (58)$$

Now let $\mathbf{Q}^e(U_n \mathbf{n} + \mathbf{U}_T^e)$ be the force vector associated with the reversible part of the displacement, which includes the normal displacement as well as the stick component of the tangential displacement, $\mathbf{U}^e = U_n \mathbf{n} + \mathbf{U}_T^e$. Since Eq. (58) is non-linear, we cannot assume that

$$\mathbf{Q}^e(U_n \mathbf{n} + \mathbf{U}_T^e) \neq \mathbf{Q}(U_n \mathbf{n} + \mathbf{U}_T^e + \mathbf{U}_T^p) - \mathbf{Q}(\mathbf{U}_T^p) \quad (59)$$

However, if the slip displacement is relatively small, the following is an acceptable first-order approximation of \mathbf{Q}

$$\begin{aligned} \mathbf{Q}(\mathbf{U}) &= \mathbf{Q}(U_n \mathbf{n} + \mathbf{U}_T^e + \mathbf{U}_T^p) \cong \mathbf{Q}(U_n \mathbf{n} + \mathbf{U}_T^e) + D\mathbf{Q} \cdot \mathbf{U}_T^p \\ &= \mathbf{Q}(\mathbf{U}^e) + \mathbf{K}(\mathbf{U}^e)\mathbf{U}_T^p \end{aligned} \quad (60)$$

A first-order approximation of the reversible traction field can therefore be obtained as

$$\mathbf{Q}(\mathbf{U}^e) = \mathbf{Q}(\mathbf{U} - \mathbf{U}_T^p) \cong \mathbf{Q}(\mathbf{U}) - \mathbf{K}(\mathbf{U}^e)\mathbf{U}_T^p \quad (61)$$

In this Eq. $\mathbf{Q}(\mathbf{U}^e)$ are the forces associated with the reversible part of the displacement, while the term $\mathbf{K}(\mathbf{U}^e)\mathbf{U}_T^p$ represents the correction needed to bring the traction field back to the Coulomb friction surface. $\mathbf{K}(\mathbf{U}^e)$ is the consistent tangent evaluated at \mathbf{U}^e .

Eq. (57) can be used in a return-mapping algorithm in a manner that is very similar to the linear small-deformation case. The term $\mathbf{Q}(\mathbf{U})$ represents the value of \mathbf{Q} obtained using the hyperplastic constitutive law and the full displacement field. The slip variables \mathbf{u}_T^p are calculated as internal variables using the following equations

$$\begin{aligned} f &= \sqrt{\mathbf{Q} \cdot \mathbf{P}\mathbf{Q}} - \mu \mathbf{Q} \cdot \mathbf{n} \\ \dot{\mathbf{u}}_T^p &= \gamma \mathbf{r}, \quad \mathbf{r} = \mathbf{P}\mathbf{Q} / \sqrt{\mathbf{Q} \cdot \mathbf{P}\mathbf{Q}} \\ \gamma &> 0, \quad f \leq 0, \quad \gamma f = 0 \end{aligned}$$

If the slip displacement is relatively large, we can modify Eq. (54) so that the linearization is performed with respect to a previously known state of the slip displacement $\mathbf{U}_T^{p,0}$

$$\mathbf{Q}(\mathbf{u}) = \mathbf{Q}(U_n \mathbf{n} + \mathbf{U}_T^e + \mathbf{U}_T^{p,0} + \Delta\mathbf{U}_T^p) \quad (62)$$

$$\begin{aligned} \mathbf{Q}(\mathbf{U}) &\cong \mathbf{Q}(U_n \mathbf{n} + \mathbf{U}_T^e + \mathbf{U}_T^{p,0}) + D\mathbf{Q} \cdot \Delta\mathbf{U}_T^p \\ &= \mathbf{Q}(\mathbf{U}^e) + \mathbf{K}(\mathbf{U}^e)\Delta\mathbf{U}_T^p \end{aligned} \quad (63)$$

leading to the modified definition of the stick force

$$\mathbf{Q}(\mathbf{U}^e) = \mathbf{Q}(U_n \mathbf{n} + \mathbf{U}_T^e + \mathbf{U}_T^{p,0}) = \mathbf{Q}(\mathbf{U} - \mathbf{U}_T^{p,0}) \cong \mathbf{Q}(\mathbf{U}) - \mathbf{K}(\mathbf{U}^e)\Delta\mathbf{U}_T^p \quad (64)$$

When discretizing Eq. (64) using the Backward Euler scheme, we can interpret the initial assumption on the slip displacement to be the value computed at the previous time step $\mathbf{U}_T^{p,0} = \mathbf{U}_{T_n}^p$. Therefore, the discretized system of equations for the Coulomb friction model becomes

$$\mathbf{U}_{n+1}^{e,trial} = \mathbf{U}_{n+1} - \mathbf{U}_{T_n}^p \quad (65)$$

$$\mathbf{Q}_{n+1}^{trial} = \mathbf{Q}(\mathbf{U}_{n+1}^{e,trial}) = \mathbf{Q}(\mathbf{U}_{n+1} - \mathbf{U}_{T_n}^p) \quad (66)$$

$$f_{n+1}^{trial} = \sqrt{\mathbf{Q}_{n+1}^{trial} \cdot \mathbf{PQ}_{n+1}^{trial}} - \mu \mathbf{Q}_{n+1}^{trial} \cdot \mathbf{n} \quad (67)$$

$$\text{If } f_{n+1}^{trial} > 0,$$

$$\mathbf{U}_{T_{n+1}}^p = \mathbf{U}_{T_n}^p + \bar{\gamma} \mathbf{r}_{n+1} \quad (68)$$

$$\mathbf{U}_{n+1}^e = \mathbf{U}_{n+1} - \mathbf{U}_{T_{n+1}}^p = \mathbf{U}_{n+1}^{e,trial} - \bar{\gamma} \mathbf{r}_{n+1} \quad (69)$$

$$\mathbf{r}_{n+1} = \frac{\mathbf{PQ}_{n+1}}{\sqrt{\mathbf{Q}_{n+1} \cdot \mathbf{PQ}_{n+1}}}, \quad \bar{\gamma} = \gamma \Delta t \quad (70)$$

$$\begin{aligned} \mathbf{Q}_{n+1}(\mathbf{U}_{n+1}^e) &\cong \mathbf{Q}(\mathbf{U}_{n+1} - \mathbf{U}_{T_n}^p) - \mathbf{K}(\mathbf{U}_{n+1}^{e,trial}) \Delta \mathbf{U}_{T_{n+1}}^p \\ &= \mathbf{Q}(\mathbf{U}_{T_n}^{e,trial}) - \bar{\gamma} \mathbf{K}(\mathbf{U}_{n+1}^{e,trial}) \mathbf{r}_{n+1} \end{aligned} \quad (71)$$

$$f_{n+1} = \sqrt{\mathbf{Q}_{n+1} \cdot \mathbf{PQ}_{n+1}} - \mu \mathbf{Q}_{n+1} \cdot \mathbf{n} = 0 \quad (72)$$

Note that the force vectors in Eqs. (66) and (71) can be computed using a hyperelastic law. The slip criterion is then computed and the tractions are updated in the same manner as the small deformation case. The consistent tangent can also be computed from Eq. (45) with the interpretation of \mathbf{K} as the instantaneous tangent at $\mathbf{U}_{n+1}^{e,trial}$.

It is useful to point out that this formulation assumes that the amount of plastic slip within a given load step is small enough for the Taylor series expansion to hold. In the case of large slip, this assumption can be satisfied using appropriately small load increments. When slip is persistent over a large number of load steps, the large total slip should be of no consequences since the value of the tangential traction should remain relatively constant as it is bounded by the slip criterion.

4. Results and discussion

In this section we show a number of numerical examples to demonstrate the effectiveness and capabilities of the proposed frictional interface formulation for large-deformation contact problems. In these examples, we will omit units in input parameters and assume consistent inputs. For example, if the modulus of elasticity is interpreted to be in *ksi*, all resulting stresses will be in *ksi* and displacements will be in *inches*. If units are assumed to be consistent, the particular choice of these units are otherwise of no influence on the numerical values of the results. For hyper-elastic materials we implement compressible Neo-Hookean material with the energy density function given by

$$\psi = \frac{\mu}{2} (I_C - 3) - \mu \ln J + \frac{\lambda}{2} (\ln J)^2,$$

where I_C is the trace of the left Green deformation tensor $\mathbf{C} = \mathbf{F}^T \mathbf{F}$, J is the determinant of the deformation gradient \mathbf{F} and $\lambda = \frac{E\nu}{(1+\nu)(1-2\nu)}$, $\mu = \frac{E}{2(1+\nu)}$ are the material Lamé parameters.

The three examples shown in this section were chosen to illustrate different aspects of the proposed implementation. The first example was chosen to challenge the simulation into switching between stick and slip states at different load levels. The second example is to verify the implementation using an example published in the literature. The third example compares

the results of the proposed approach to those obtained using Abaqus with the updated Lagrangian method.

Example 1

The first example represents a simple configuration of a punch sitting atop an elastic foundation as shown in Fig. 8. The two bodies have the same modulus of elasticity of 30,000 and Poisson's ratio of 0.3. A vertical pressure $P = 200$ and a prescribed horizontal displacement $u = 0.04$ are applied to the top punch as shown in Fig. 8. The loads were applied in nine increments, assuming large deformations and a Coulomb frictional coefficient of 0.4 is used. The contact constraints are enforced using Lagrange multipliers and the proposed stick-slip formulation is applied to the interface.

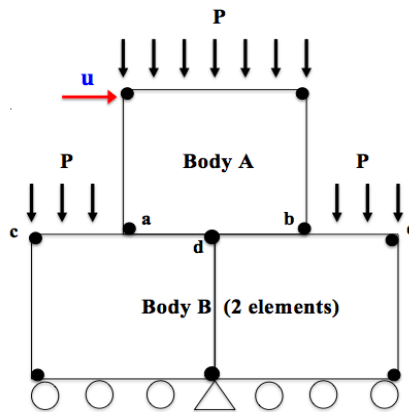


Fig. 8 Sliding Patch Test

Fig. 9 shows the deformed shapes at each load increment. The results show that node 1 (bottom left corner of Body A) is slipping while node 2 (bottom right corner of Body A) is sticking along the interface. The two states were handled in an equally efficient manner, with few (<5) iterations using the Newton method and without the need to repeat the overall nonlinear solution to revise an assumption on stick or slip. These results showcase the capability of the proposed frictional interface formulation in handling both the stick and slip conditions.

Example 2

The second numerical example is obtained from Simo and Laursen (1992) and is used to verify the implementation of the stick-slip decomposition framework for friction for the case of linear elasticity with small deformations. The example considers an elastic block sitting on a rigid foundation and subjected to a normal pressure field on its top surface while being pulled tangentially by a lateral traction applied to its right edge, as shown in Fig. 10. The block has an elastic modulus of 1,000 and Poisson's ratio of 0.3, and the Coulomb friction coefficient on the block-foundation interface is $\mu = 0.5$. To follow the exact conditions used by the authors in this paper, no frictional stress is allowed to develop at the first and last nodes of the contact surface due to the uplifting at the edges. Therefore, these ends are assumed not to be in contact with the foundation. The rigid foundation is modeled with solid elements with a very high modulus of elasticity.

The resulting deformed shape shown in Fig. 11 is in agreement with the results reported by

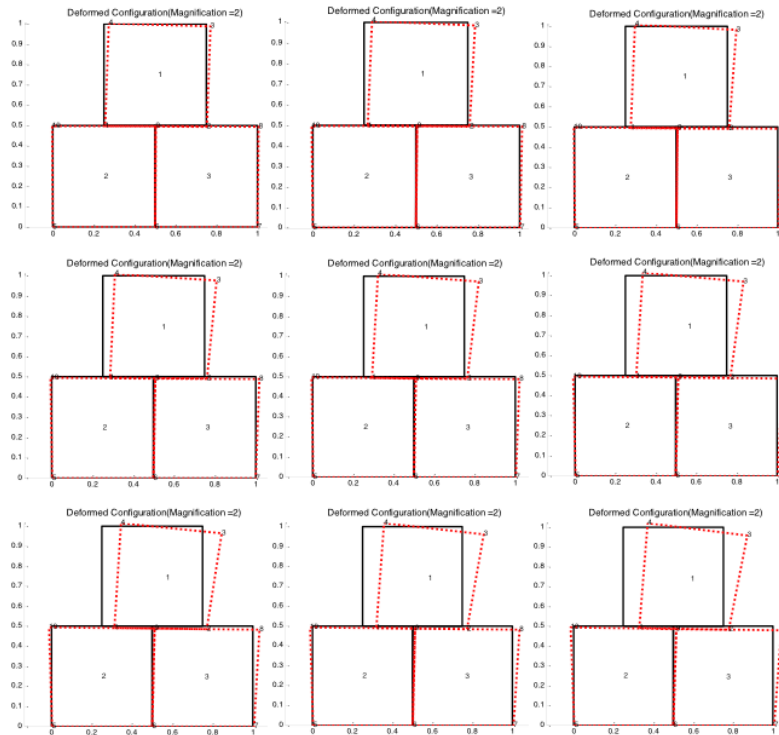


Fig. 9 Incremental Deformation in a Punch-Foundation System (Example 1)

Simo and Laursen (1992) and shows the block being compressed under the normal loading and pulled to the right as a result of the horizontal load. The deformation shape also confirms the assumption of uplift at the corner nodes and is identical to the one reported in the reference. Fig. 12 shows the distribution of vertical and horizontal axial stresses in the elastic block and foundation, in which high stress values are observed along the edges closest to the applied loads, as would be expected. It is useful to point out that the mesh chosen in this simulation is identical to the one reported by Simo and Laursen in order to maintain comparability of the results.

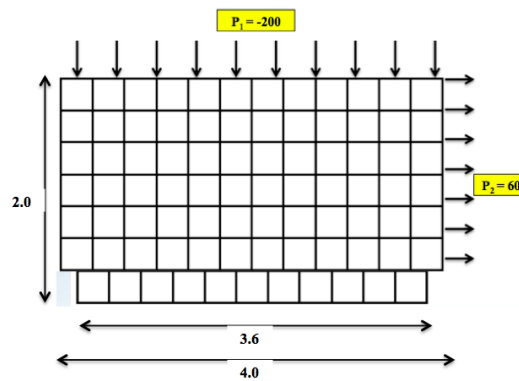


Fig. 10 Geometry and Loading Conditions for Example 2

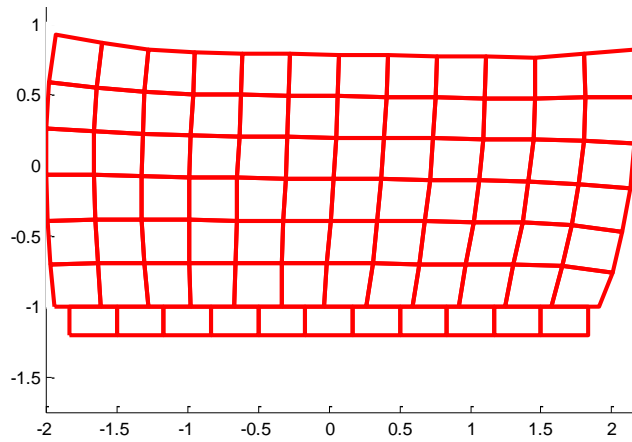


Fig. 11 Deformed Shape for Example 2

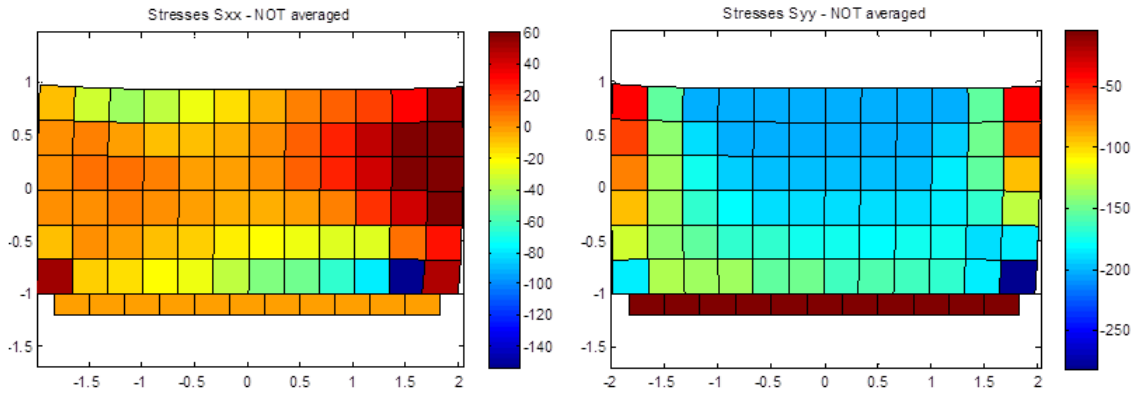


Fig. 12 Axial Stresses Distribution for Example 2

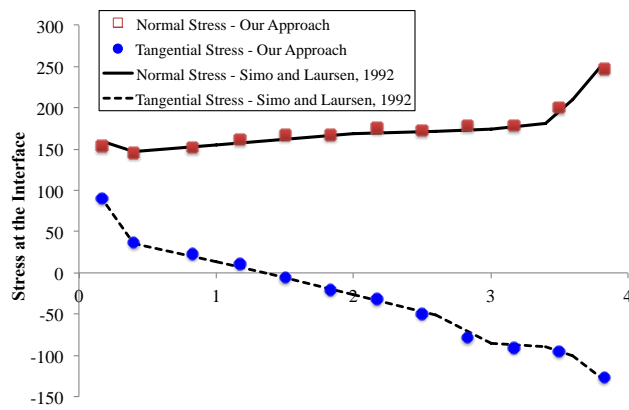


Fig. 13 Interface Tangential and Normal Stresses for Example 2

The distribution of normal and tangential interface stresses is compared with the results of Simo and Laursen in Fig. 13. Since the proposed formulation is based on nodal forces, and for a

consistent comparison with the stress results of Simo and Laursen, interface stresses were computed from the nodal forces vector by normalizing with respect to element length. Both the normal and tangential tractions show perfect agreement.

Example 3

In this example we simulate the frictional contact between two hyperelastic bodies with the configuration shown in Fig. 14. This example consists of two hyperelastic bodies, 1 and 2, with geometric dimensions $AC=CE=EF=FA=IH=JG=3$, $IJ=HG=9$. Body 1 is subjected to a normal pressure of 90 and a prescribed lateral displacement $u=5$. The two bodies have different material properties, with Young's modulus values of 3000 and 100000, and Poisson's ratio of 0.3 and 0, in Body 1 and 2, respectively. The Coulomb friction coefficient for the interface is 0.4.

Figs. 15 and 16 show the distribution of the resulting horizontal and vertical axial stresses in the bodies 1 and 2. The results show that the values are higher at locations closest to the applied loads, and the results also show a good agreement with ABAQUS. The computed interface tractions are shown in Fig. 17. and the comparison shows matching results with ABAQUS. While the Abaqus solution oscillated between stick and slip states, the solution using the proposed approach suffered no such oscillations. The number of global iterations is reduced by an estimated 50% since the solution at each step does not need to be repeated with changes in stick/slip conditions. Greater savings are expected in larger systems.

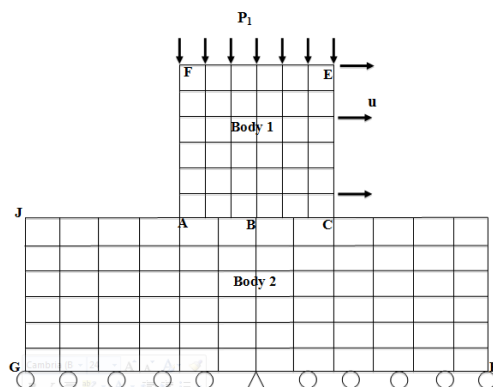


Fig. 14 Geometry and Loading Conditions for Example 3

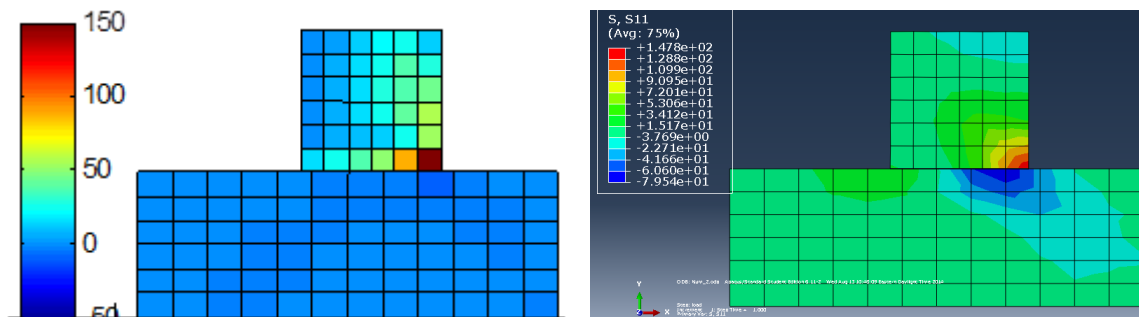


Fig. 15 Horizontal Axial Stress Distribution for Numerical Example 3: Proposed Approach (left) versus ABAQUS (right)

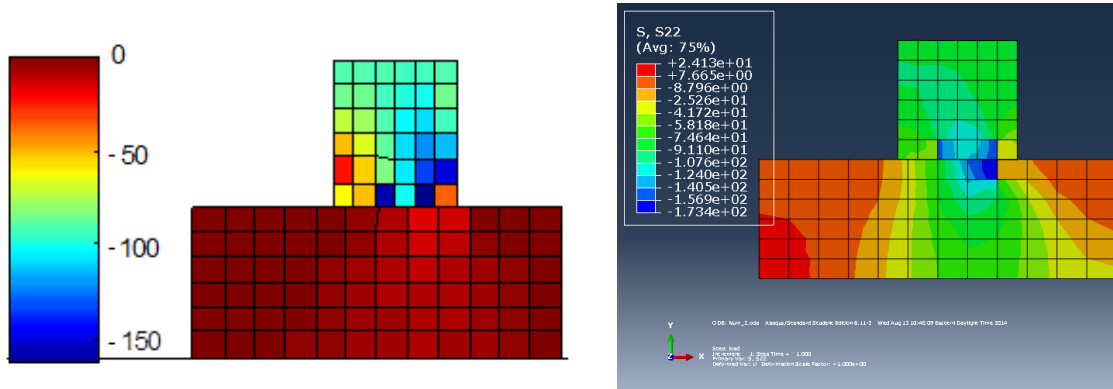


Fig. 16 Vertical Axial Stress Distribution for Example 3: Proposed (left) versus ABAQUS (right)

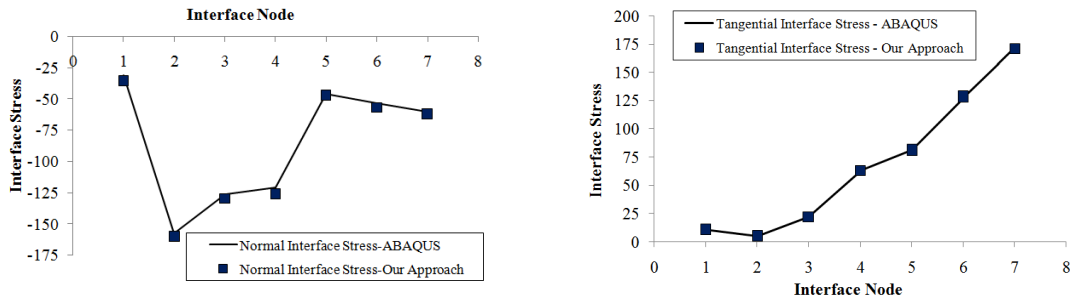


Fig. 17 Tangential and Normal Traction Components along the Interface for Example 3

5. Conclusions

Methods used to enforce Coulomb frictional contact conditions pose a major algorithmic challenge due to the inability of the algorithm to handle transitions between stick and slip states at contact points smoothly. Each change in stick/slip condition requires the repetition of the Newton solution for the whole problem, a process that could prove costly in large meshes. Oscillations between stick and slip states could be the cause of algorithm instability, often leading to ill-conditioning and non-convergence of the solution.

To remedy this problem, a new plasticity-inspired, stick-slip decomposition method for handling frictional conditions under large deformations is introduced. The proposed approach is designed to increase algorithmic efficiency and circumvent numerical issues encountered when modeling stick/slip conditions in Coulomb frictional contact models. The method is based on an additive decomposition of the displacement at the contact interface into “stick” and “slip” components, with the latter following a non-associative flow rule based on the slip criterion defined by the Coulomb friction model. A linearization of interface tractions around a “stick” state ensures the applicability of this approach to the case of material and geometric nonlinearity. The approach produces accurate results that compare well with those obtained using available techniques at a reduced computational cost.

References

- Alart, P. and Curnier, A. (1991), "A mixed formulation for frictional contact problems prone to Newton like solution methods", *Comput. Meth. Appl. Mech. Eng.*, **92**, 353-375.
- Baillet, L. and Sassi, T. (2005), "Mixed finite element formulation in large deformation frictional contact problem", *Revue Eur. des Élé. Fin.*, **14**(2-3), 287-304.
- Bonnet, J. and Wood, R.D. (2008), *Nonlinear Continuum Mechanics for Finite Element Analysis*, 2nd Edition, Cambridge.
- Burman, E., Hansbo, P. and Larson, M.G. (2017), *Augmented Lagrangian and Galerkin Least Squares Methods for Membrane Contact*, arXiv: 1711.04494.
- Bussetta, P., Marceau, D. and Ponthot, J.P. (2012), "The adapted augmented Lagrangian method: A new method for the resolution of the mechanical frictional contact problem", *Comput. Mech.*, **49**(2), 259-275.
- Chouly, F., Mlika, R. and Renard, Y. (2018), "An unbiased Nitsche's approximation of the frictional contact between two elastic structures", *Numer. Mathemat.*, **139**(3), 593-631.
- De Saxcé, G. and Feng, Z.Q. (1998), "The bipotential method: A constructive approach to design the complete contact law with friction and improved numerical algorithms", *Math. Comput. Modell.*, **28**(4-8), 225-245.
- Fischer, K.A. and Wriggers, P. (2006), "Mortar based frictional contact formulation for higher order interpolations using the moving friction cone", *Comput. Meth. Appl. Mech. Eng.*, **195**, 5020-5036.
- Gálvez, J., Cardona, A., Cavalieri, F. and Brüls, O. (2017), "An augmented Lagrangian frictional contact formulation for nonsmooth multibody systems", *Proceedings of the ENOC 2017*, Budapest, Hungary.
- Gholami, F., Nasri, M., Kövecses, J. and Teichmann, M. (2016), "A linear complementarity formulation for contact problems with regularized friction", *Mech. Mach. Theory*, **105**, 568-582.
- Gu, Q., Barbato, M. and Conte, J.P. (2009), "Handling of constraints in finite-element response sensitivity analysis", *ASCE J. Eng. Mech.*, **135**(12), 1427-1438.
- Hild, P. and Renard, Y. (2010), "A stabilized lagrange multiplier method for the finite element approximation of contact problems in elastostatics", *Numer. Math.*, **115**, 101-129.
- Ibrahimbegovic A. and Wilson, E.L. (1991), "Unified computational model for static and dynamic frictional contact analysis", *Int. J. Numer. Meth. Eng.*, **34**, 233-247.
- Ibrahimbegovic, A. (2009), *Nonlinear Solid Mechanics: Theoretical Formulations and Finite Element Solution Methods*, Springer.
- Laursen, T.A. and Simo, J.C. (1993a), "Algorithmic symmetrization of coulomb frictional problems using augmented Lagrangians", *Comput. Meth. Appl. Mech. Eng.*, **108**(1-2), 133-146.
- Laursen, T.A. and Simo J.C. (1993b), "A continuum-based finite element formulation for the implicit solution of multibody, large-deformation frictional contact problems", *Int. J. Numer. Meth. Eng.*, **36**(20), 3451-3485.
- McDevitt, T.W. and Laursen, T.A. (2000), "A mortar-finite element formulation for frictional contact problems", *Int. J. Numer. Meth. Eng.*, **48**, 1525-1547.
- Masud, A., Truster, T.J. and Bergman, L.A. (2012), "A unified formulation for interface coupling and frictional contact modeling with embedded error estimation," *Int. J. Numer. Meth. Eng.*, **92**(2), 141-177.
- Mlika, R., Renard, Y. and Chouly, F. (2017), "An unbiased Nitsche's formulation of large deformation frictional contact and self-contact", *Comput. Meth. Appl. Mech. Eng.*, **325**, 265-288.
- Pietrzak, G. and Curnier, A. (1999), "Large-deformation frictional contact mechanics: Continuum formulation and augmented Lagrangian treatment", *Comput. Meth. Appl. Mech. Eng.*, **177**(3-4), 351-381.
- Popp, A., Wohlmuth, B.I., Gee, M.W. and Wall, W.A. (2012), "Dual quadratic mortar finite element methods for 3D finite deformation contact", *SIAM J. Sci. Comput.*, **34**(4), B421-B446.
- Puso, M.A. and Laursen, T.A. (2004), "A mortar segment-to-segment contact method for large deformation solid mechanics", *Comput. Meth. Appl. Mech. Eng.*, **193**, 601-629.
- Sheng, D., Wriggers, P. and Sloan, S.W. (2006), "Improved numerical algorithms for frictional contact in pile penetration analysis", *Comput. Geotech.*, **33**(6-7), 341-354.

- Sheng, D., Wriggers, P. and Sloan, S.W. (2007), "Application of frictional contact in geotechnical engineering", *Int. J. Geomech.*, **7**(3), 176-185.
- Sheng, D., Yamamoto, H. and Wriggers, P. (2008), "Finite element analysis of enlarged end piles using frictional contact", *Soils Foundat. Jap. Geotech. Soc.*, **48**(1), 1-14.
- Simo, J.C., Taylor, R.L. and Pister, K.S. (1985), "Variational and projection methods for the volume constraint in finite-deformation elasto-plasticity", *Comput. Meth. Appl. Mech. Eng.*, **51**, 177-208.
- Simo, J.C. and Laursen, T.A. (1992), "An augmented Lagrangian treatment of contact problems involving friction", *Comput. Struct.*, **42**(1), 97-116.
- Ștefancu, A.I., Melenciuc, S.C. and Budescu, M. (2011), "Penalty based algorithms for frictional contact problems", *Bullet. Polytech. Inst. Iasi-Constr. Architect.*, **61**(3), 119.
- Terfaya, N., Berga, A. and Raous, M. (2015), "A bipotential method coupling contact, friction and adhesion", *Int. Rev. Mech. Eng.*, **9**(4).
- Vulovic, S., Zivkovic, M., Grujovic, N. and Slavkovic, R. (2007), "A comparative study of contact problems solution based on the penalty and lagrange multiplier approaches", *J. Serb. Soc. Comput. Mech.*, **1**(1), 174-183.
- Wriggers, P. (2006), *Computational Contact Mechanics*, 2nd Edition, Springer.
- Wriggers, P. and Zavarise, G. (1993), "On the application of augmented Lagrangian techniques for nonlinear constitutive laws in contact interfaces," *Commun. Numer. Meth. Eng.*, **9**(10), 815-824.